# Core polarization for the electric quadrupole moment of neutron-rich aluminum isotopes

Kenichi Yoshida

*RIKEN Nishina Center for Accelerator-Based Science, Wako, Saitama 351-0198, Japan*

The core polarization effects for the electric quadrupole moments of the neutron-rich $^{31}$Al, $^{33}$Al, and $^{35}$Al isotopes in the vicinity of the island of inversion are investigated by means of the microscopic particle-vibration coupling model in which the Skyrme Hartee-Fock-Bogoliubov and quasiparticle random-phase approximations are used to calculate the single-quasiparticle wave functions and the excitation modes. It is found that the polarization charge for the proton $1d_{5/2}$ hole state in $^{33}$Al is quite sensitive to coupling to the neutrons in the $pf$-shell associated with the pairing correlations and that the polarization charge in $^{35}$Al becomes larger due to the stronger collectivity of the low-lying quadrupole vibrational mode in the neighboring $^{36}$Si nucleus.

## I. INTRODUCTION

The nuclear structure far from the $\beta$-stability line has been studied very actively with the development of the new generation radioactive-isotope beam techniques together with the microscopic nuclear models applicable to drip-line nuclei carried out by high performance computers.

The ground state properties and the dynamical properties such as low-energy excitation modes and giant resonances in the medium-mass nuclei to the heavier nuclei have been successfully described by the self-consistent mean-field theory or the nuclear density-functional theory (DFT) [1]. The nuclear DFT has been applied to the exotic modes of excitation in unstable nuclei [2,3] and developed toward description of nuclei in the whole chart. Along this line, the self-consistent random-phase approximation (RPA) including the pairing correlation and the nuclear deformation has been recently developed by several groups [4–6].

Presently, the small excitation energy of the $2_1^+$ state and the large transition probability $B(E2; 0^+ \rightarrow 2_1^+)$ in $^{32}$Mg have been discussed in connection with the breaking of the spherical magic number $N = 20$ in neutron-rich systems [7–9]. The recent gyromagnetic-factor measurement of $^{33}$Al at GANIL [10] and the $\beta$-decay study of $^{33}$Mg at NSCL [11] indicate that $^{33}$Al has a certain amount of 2p-2h intruder configuration.

The electric quadrupole moment ($Q$ moment) representing the deviation from a sphere is directly related to the deformation property of the nucleus, and thus its investigation for neutron-rich nuclei at around $N = 20$ is strongly desired both experimentally and theoretically [12]. Quite recently, the $Q$-moment measurement of $^{33}$Al has been performed at GANIL [13].

To investigate the ground-state $Q$ moments of neutron-rich Al isotopes in the vicinity of the "island of inversion" [14], we carry out the particle-vibration coupling (PVC) calculation based on the Skyrme energy-density functional, on top of the self-consistent quasiparticle RPA (QRPA).

The article is organized as follows. In Sec. II, the method is explained. In Sec. III, we perform the numerical calculations and investigate the core polarization for the electric quadrupole moments in $^{31,33,35}$Al. Section IV contains the conclusions.

## II. METHOD

### A. Microscopic particle-vibration coupling model

The nuclear Hamiltonian of a PVC model [15] on top of the Skyrme Hartree-Fock-Bogoliubov (HFB) and QRPA is written as

$$\hat{H} = \sum_i E_i \hat{\beta}_i^\dagger \hat{\beta}_i + \sum_\lambda \hbar\omega_\lambda \hat{B}_\lambda^\dagger \hat{B}_\lambda + \hat{H}_{\text{couple}}. \quad (1)$$

Here $E_i$ is the quasiparticle energy obtained as a self-consistent solution of the Skyrme HFB equation and $\hat{\beta}_i^\dagger$ and $\hat{\beta}_i$ are the quasiparticle creation and annihilation operators. The nucleon creation operator $\hat{\psi}^\dagger(\mathbf{r})$ is then represented, using the quasiparticle wave functions, as

$$\hat{\psi}^\dagger(\mathbf{r}) = \sum_i \varphi_{1,i}(\mathbf{r})\hat{\beta}_i^\dagger + \varphi_{2,i}^*(\mathbf{r})\hat{\beta}_i. \quad (2)$$

The phonon energy $\hbar\omega_\lambda$ is a solution of the QRPA equation on top of the Skyrme HFB, and $\hat{B}_\lambda^\dagger$ and $\hat{B}_\lambda$ are the phonon creation and annihilation operators. We solve the Skyrme HFB + QRPA equations in the $m$ scheme. Details of the calculation scheme are given in Ref. [6].

Let us now consider the change of the density $\varrho(\mathbf{r})$ due to the collective vibrations as $\varrho(\mathbf{r}) \rightarrow \varrho(\mathbf{r}) + \delta\varrho(\mathbf{r}, t)$. The nuclear potential $U[\varrho(\mathbf{r})]$ is accordingly changed to $U[\varrho(\mathbf{r})] \rightarrow U[\varrho(\mathbf{r}) + \delta\varrho(\mathbf{r}, t)]$. To first order in the change of the density, the difference of the nuclear potential is evaluated to be

$$U[\varrho(\mathbf{r}) + \delta\varrho(\mathbf{r}, t)] - U[\varrho(\mathbf{r})] = \int d\mathbf{r}' \frac{\delta U[\varrho(\mathbf{r})]}{\delta\varrho(\mathbf{r}')} \delta\varrho(\mathbf{r}', t). \quad (3)$$

Then, the PVC Hamiltonian has the form

$$\hat{H}_{\text{couple}} = \int d\mathbf{r} d\mathbf{r}' \frac{\delta U[\varrho(\mathbf{r})]}{\delta\varrho(\mathbf{r}')} \delta\varrho(\mathbf{r}', t)\hat{\psi}^\dagger(\mathbf{r})\hat{\psi}(\mathbf{r}). \quad (4)$$

We introduce the vacuum defined by the product of the HFB vacuum and the QRPA vacuum:

$$\hat{\beta}_i|0\rangle = 0, \quad \hat{B}_\lambda|0\rangle = 0. \quad (5)$$

The density variation $\delta\varrho(\mathbf{r}, t)$ can be written in a second quantized form, using the QRPA modes, as

$$\delta\hat{\varrho}(\mathbf{r}) = \sum_\lambda [\delta\varrho_\lambda(\mathbf{r})\hat{B}_\lambda^\dagger + \delta\varrho_\lambda^*(\mathbf{r})\hat{B}_\lambda], \qquad (6)$$

where $\delta\varrho_\lambda(\mathbf{r})$ is a transition density to the QRPA state $|\lambda\rangle = \hat{B}_\lambda^\dagger|0\rangle$.

The $\hat{\beta}_i^\dagger\hat{\beta}_j^\dagger$ and $\hat{\beta}_j\hat{\beta}_i$ parts in $\psi^\dagger(\mathbf{r}')\psi(\mathbf{r})$ are taken into account in the QRPA phonons [16]. Consequently, the PVC Hamiltonian in the leading order reads

$$\hat{H}_{\text{couple}} = \sum_{\lambda,ij} \int d\mathbf{r} d\mathbf{r}' \frac{\delta U[\varrho(\mathbf{r})]}{\delta\varrho(\mathbf{r}')} [\delta\varrho_\lambda(\mathbf{r}')\hat{B}_\lambda^\dagger + \delta\varrho_\lambda^*(\mathbf{r}')\hat{B}_\lambda]$$
$$\times [\varphi_{1,i}(\mathbf{r})\varphi_{1,j}^*(\mathbf{r}) - \varphi_{2,i}(\mathbf{r})\varphi_{2,j}^*(\mathbf{r})]\beta_i^\dagger\beta_j. \qquad (7)$$

The higher order effects can be treated systematically in the Nuclear Field Theory [17,18].

The coupling interaction in Eq. (7) is derived from the Skyrme energy-density functional. In the present calculation, we approximate the momentum-dependent terms in the Skyrme interaction by the Landau-Migdal (LM) form. This approximation is made only for the construction of the PVC Hamiltonian as in Refs. [19] and [20]. The isoscalar (IS) and the isovector (IV) coupling interactions are expressed as

$$\frac{\delta U[\varrho(\mathbf{r})]}{\delta\varrho(\mathbf{r}')}\delta\varrho_\lambda(\mathbf{r}') = \begin{cases} v^{\tau=0}(\mathbf{r})\delta\varrho_\lambda^{\text{IS}}(\mathbf{r}')\delta(\mathbf{r} - \mathbf{r}') \\ v^{\tau=1}(\mathbf{r})\delta\varrho_\lambda^{\text{IV}}(\mathbf{r}')\delta(\mathbf{r} - \mathbf{r}')\tau_z\tau_z'. \end{cases} \qquad (8)$$

The explicit expressions for $v^{\tau=0}(\mathbf{r}) = F_0/N_0$ and $v^{\tau=1}(\mathbf{r}) = F_0'/N_0$ are given in Ref. [21].

### B. Description of odd-$A$ systems

To describe the odd-$A$ nuclear systems, we diagonalize the Hamiltonian (1) within the subspace $\{\hat{\beta}_i^\dagger|0\rangle, \hat{B}_\lambda^\dagger\hat{\beta}_j^\dagger|0\rangle\}$. Then, the resulting state vector is written as

$$|\phi\rangle = \sum_i c_i^0\hat{\beta}_i^\dagger|0\rangle + \sum_{\lambda j} c_{\lambda j}^1\hat{B}_\lambda^\dagger\hat{\beta}_j^\dagger|0\rangle. \qquad (9)$$

The operator for the quadrupole moment can be written as

$$\hat{Q} = \langle\hat{Q}\rangle + \sum_{ij\in\pi} Q_{ij}\hat{\beta}_i^\dagger\hat{\beta}_j + \sum_\lambda (Q_\lambda\hat{B}_\lambda^\dagger + Q_\lambda^*\hat{B}_\lambda), \quad (10)$$

where

$$Q_{ij} = \langle 0|\hat{\beta}_i\hat{Q}\hat{\beta}_j^\dagger|0\rangle$$
$$= \int d\mathbf{r}(3z^2 - r^2)[\varphi_{1,i}(\mathbf{r})\varphi_{1,j}^*(\mathbf{r}) - \varphi_{2,i}(\mathbf{r})\varphi_{2,j}^*(\mathbf{r})],$$

$$\qquad\qquad\qquad (11a)$$

$$Q_\lambda = \langle 0|[\hat{B}_\lambda, \hat{Q}]|0\rangle = \int d\mathbf{r}(3z^2 - r^2)\delta\varrho_\lambda^\pi(\mathbf{r}), \qquad (11b)$$

and $\langle\hat{Q}\rangle$ is the vacuum expectation value.

The electric $Q$ moment of the eigenstate $|\phi\rangle$ is then calculated as

$$\langle\phi|e\hat{Q}|\phi\rangle = e\left\{\langle\hat{Q}\rangle + \sum_i \left[(c_i^0)^2 Q_{ii} + 2c_i^0\sum_\lambda c_{\lambda i}^1 Q_\lambda\right]\right.$$
$$\left. + \sum_{\lambda,jk} c_{\lambda j}^1 c_{\lambda k}^1 Q_{jk}\right\}. \qquad (12)$$

We apply this model to odd-$Z$ nuclei to calculate the proton polarization charge of the state $|i\rangle$ for the $Q$ moment, which is defined as

$$e_{\text{pol}}^\pi = e\left(\frac{\langle\phi|\hat{Q}|\phi\rangle}{\langle i|\hat{Q}|i\rangle} - 1\right), \qquad (13)$$

where $\langle i|\hat{Q}|i\rangle = \langle\hat{Q}\rangle + Q_{ii}$.

### C. Parameters

For the mean-field Hamiltonian, we employ the SkM* interaction [22] in the present numerical applications. We use the lattice mesh size $\Delta\rho = \Delta z = 0.6$ fm and a box boundary condition at ($\rho_{\max} = 9.9$ fm, $z_{\max} = 9.6$ fm). The quasiparticle energy cutoff is chosen at $E_{\text{qp,cut}} = 60$ MeV and the quasiparticle states up to $\Omega^\pi = 15/2^\pm$ are included. The pairing strength parameter is determined so as to reproduce the experimental pairing gap for neutrons in $^{34}$Mg($\Delta_{\text{exp},\nu} = 1.7$ MeV) obtained by the three-point formula [23]. The strength $t_0' = -295$ MeV fm$^3$ for the mixed-type pairing interaction with the exponent of the density dependence $\gamma = 1$ leads to the pairing gap $\langle\Delta_\nu\rangle = 1.71$ MeV in $^{34}$Mg [6]. On top of the Skyrme HFB, we solve the QRPA equation within the space of the two-quasiparticle excitation of $E_\alpha + E_\beta \leqslant 60$ MeV. The momentum-dependent terms in the residual interaction are exactly treated.

The density-dependent Landau parameters $F_0$ and $F_0'$ for the PVC interaction are determined by the parameters of the SkM* interaction. As shown in Refs. [6] and [24], the attraction of the LM interaction is stronger than that of the self-consistent interaction in which the momentum-dependent terms are treated exactly. In the case of $^{20}$O in Ref. [6], we needed an overall factor $f_{\text{LM}} = 0.82$ for the residual interaction to obtain the spurious mode at zero energy. Therefore, we multiply the overall factor $f_{\text{LM}}$ for the PVC interaction. We use $f_{\text{LM}} = 0.8$ and 0.9 for comparison. Accordingly, the difference of the results can be considered as a theoretical uncertainty.

## III. RESULTS AND DISCUSSION

### A. Properties of $^{32,34,36}$Si

We describe the odd-$Z$ neutron-rich Al isotopes as a proton single-hole state coupled to the neighboring Si isotopes because the pairing gaps of protons in Si isotopes are zero. We summarize here the ground state properties and the structure of quadrupole excitations in $^{32,34,36}$Si.

TABLE I. Ground state properties of $^{32,34,36}$Si obtained by the deformed HFB calculation with the SkM* interaction and the mixed-type pairing interaction. Chemical potentials, average pairing gaps, and root-mean-square radii for neutrons and protons are listed. The average pairing gap of protons is zero in these isotopes. The average pairing gap is defined as $\langle\Delta\rangle_q = -\int d\mathbf{r}\,\tilde{h}\tilde{\varrho}/\int d\mathbf{r}\,\tilde{\varrho}$.

|  | $^{32}$Si | $^{34}$Si | $^{36}$Si |
|---|---|---|---|
| $\lambda_\nu$ (MeV) | $-7.76$ | $-6.60$ | $-5.51$ |
| $\lambda_\pi$ (MeV) | $-13.5$ | $-15.9$ | $-17.3$ |
| $\langle\Delta\rangle_\nu$ (MeV) | $1.56$ | $1.67$ | $1.94$ |
| $\sqrt{\langle r^2\rangle_\nu}$ (fm) | $3.22$ | $3.32$ | $3.39$ |
| $\sqrt{\langle r^2\rangle_\pi}$ (fm) | $3.10$ | $3.13$ | $3.16$ |

In Table I, the ground state properties are summarized. The neutron-rich Si isotopes under investigation are spherical although the calculated deformation parameters are not exactly zero ($\beta_2 = 0.02$ in $^{34}$Si). This is due to the artificial breaking of the spherical symmetry associated with the finite mesh size and the rectangular box, and thus it is considered as a numerical error. The average pairing gaps of neutrons are finite, while those of protons are zero. This indicates that the $^{34}$Si has a neutron 2p-2h configuration in its ground state. The neutron occupation numbers of the $1f_{7/2}$ orbital are 0.31, 0.78, and 2.21 in $^{32,34,36}$Si, respectively, and the neutron occupation number of the $2p_{3/2}$ orbital is 0.10 in $^{36}$Si.

Figure 1 shows the response functions for the isoscalar (IS), isovector (IV), and proton quadrupole excitations. We can see a prominent peak at around 3 MeV in all of the isotopes under investigation. The isoscalar transition strengths are $B(IS2; 0^+ \to 2_1^+) = 626$, 637, and 1137 fm$^4$ in $^{32,34,36}$Si,
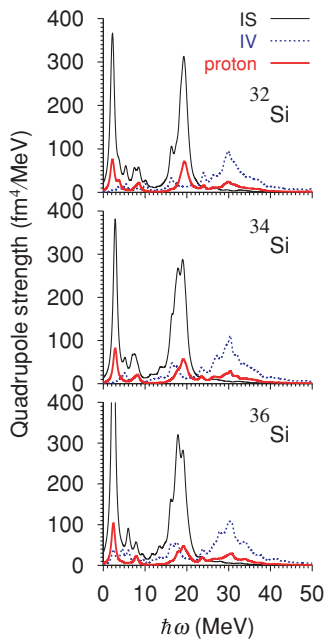


FIG. 1. (Color online) Response functions for the isoscalar (IS), isovector (IV), and proton quadrupole excitations in $^{32,34,36}$Si. The transition strengths are smeared by a Lorentzian function with a width of $\Gamma = 1$ MeV.
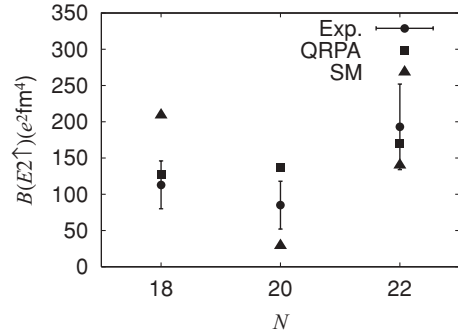


FIG. 2. $B(E2; 0^+ \to 2_1^+)$ values of Si isotopes as functions of neutron numbers. The calculated values (QRPA) are compared with the MCSM results [25] (SM) and the experimental results [26] (Exp.).

corresponding to 104, 98, and 162 in Weisskopf units. In addition to the low-lying collective $2^+$ state, we can see the giant quadrupole resonances (GQR) at around 20 and 30 MeV for the IS and IV excitations.

The calculated $B(E2; 0^+ \to 2_1^+)$ values are shown in Fig. 2 and compared with the Monte-Carlo Shell Model (MCSM) results [25] and the experimental values [26]. The present results agree reasonably with the experimental results. Furthermore, the shell model calculation in the full $sdpf$ space performed in Ref. [28] gives a larger $B(E2)$ value of 118 $e^2$ fm$^4$ in $^{34}$Si, which is closer to the present result. And the present calculation gives the same result as that obtained in Ref. [29] employing the spherical HFB-QRPA model for $^{34}$Si.

The $2_1^+$ state in $^{32}$Si is mainly generated by the $sd$-shell configurations of neutrons and protons. The microscopic structure of the $K^\pi = 0^+$ component is given by the two-quasiparticle excitations of $(\nu 2s_{1/2} \otimes 1d_{3/2})$ with a weight of 0.04, $(\nu 1d_{3/2})^2$ with 0.61, and $(\pi 2s_{1/2} \otimes 1d_{5/2})$ with 0.30. The microscopic structure of the $K^\pi = 1^+$ and $2^+$ components is the same within the numerical accuracy as that of the $K^\pi = 0^+$ component because of the spherical symmetry. The strength in the energy region $15 \leqslant \hbar\omega \leqslant 25$ MeV exhausts 79.4% of the IS energy-weighted sum rule (EWSR) value. The IS strength in the low-energy region up to 10 MeV exhausts 1.2% of EWSR. The IV strength is distributed in a wider energy range, $20 \leqslant \hbar\omega \leqslant 40$ MeV. The summed strength in this energy region exhausts 75.2% of the IV-EWSR value.

In $^{34}$Si the neutron excitations into the $pf$-shell become appreciable for the $2_1^+$ state. The microscopic structure of the $K^\pi = 0^+$ component is given by the $(\nu 1d_{3/2})^2$ excitation with a weight of 0.21, the $(\nu 1f_{7/2})^2$ excitation with 0.10, and the $(\pi 2s_{1/2} \otimes 1d_{5/2})$ excitation with 0.63. The strength in the energy region $15 \leqslant \hbar\omega \leqslant 25$ MeV exhausts 79.8% of the IS-EWSR value, and the strength in the energy region $20 \leqslant \hbar\omega \leqslant 40$ MeV exhausts 74.3% of the IV-EWSR value.

The $K^\pi = 0^+$ component of the $2_1^+$ state in $^{36}$Si is mainly generated by the $(\nu 1f_{7/2})^2$ excitation with a weight of 0.39, the $(\nu 2p_{3/2})^2$ excitation with 0.08, and the $(\pi 2s_{1/2} \otimes 1d_{5/2})$ excitation with 0.47. The strength in the energy region $15 \leqslant \hbar\omega \leqslant 25$ MeV exhausts 77.6% of the IS-EWSR value, and the strength in the energy region $20 \leqslant \hbar\omega \leqslant 40$ MeV exhausts 72.9% of the IV-EWSR value. Because of the mixing of the IS and IV modes in neutron-rich nuclei, we can see an

appreciable IV strength in the lower energy region $10 \leqslant \hbar\omega \leqslant 20$ MeV. The summed strength in this energy region exhausts 10.4% of the IV-EWSR value.

### B. Polarization charges in $^{31,33,35}$Al

For describing the $I^{\pi} = 5/2^+$ state of $^{31,33,35}$Al, we diagonalize the Hamiltonian (1) in the model space of the proton single-hole state of the $1d_{5/2}$ orbital $|(\Omega^{\pi} = -5/2^+)^{-1}\rangle$ and the coupled states of $|(\Omega^{\pi} = -5/2^+)^{-1} \otimes \omega_{K=0}\rangle$, $|(-3/2^+)^{-1} \otimes \omega_{K=1}\rangle$, and $|(-1/2^+)^{-1} \otimes \omega_{K=2}\rangle$. We take the QRPA states $|\omega_{\lambda}\rangle$ whose IS or IV quadrupole transition strengths possess greater than 1 W.u.

The dimension of the Hamiltonian (1) is 225 for $^{31}$Al. The $I^{\pi} = 5/2^+$ state of $|^{31}$Al$\rangle$ is constructed mainly by the one-hole state and the hole coupled to the $2_1^+$ state as

$$
\begin{aligned}
|^{31}\text{Al}; I^{\pi} = 5/2^+, M = 5/2\rangle ={}& 0.93|(-5/2^+)^{-1}\rangle \\
&+ 0.21|(-5/2^+)^{-1} \otimes 2_1^+(K=0)\rangle \\
&- 0.23|(-3/2^+)^{-1} \otimes 2_1^+(K=1)\rangle \\
&+ 0.16|(-1/2^+)^{-1} \otimes 2_1^+(K=2)\rangle. \quad (14)
\end{aligned}
$$

The amplitudes associated with the other components are smaller than 0.1. The coupled states in Eq. (14) correspond to the $|(\pi 1d_{5/2})^{-1} \otimes 2_1^+\rangle$ state in the $j$-scheme representation. The ratios of the amplitudes are identical to those of the Clebsch-Gordan coefficients $\langle \frac{5}{2}\frac{5}{2}20|\frac{5}{2}\frac{5}{2}\rangle$, $\langle \frac{5}{2}\frac{3}{2}21|\frac{5}{2}\frac{5}{2}\rangle$, and $\langle \frac{5}{2}\frac{1}{2}22|\frac{5}{2}\frac{5}{2}\rangle$. The quadrupole moment of $^{31}$Al is then calculated using Eq. (12) as $13.6(13.9)e$ fm$^2$, where we use $f_{\text{LM}} = 0.8$ (0.9). From this value, the polarization charge of Eq. (13) is calculated as $e_{\text{pol}}^{\pi} = 1.03e$ (1.08$e$). The result of the calculation overestimates slightly the experimental value of the $Q$ moment $11.2 \pm 3.2e$ fm$^2$ [12].

For $^{33}$Al, the dimension of the Hamiltonian (1) is 250. As in $^{31}$Al, the wave function of $^{33}$Al is written mainly by the one-hole state with a weight (the squared amplitude) of 0.90 and the hole coupled to the $2_1^+$ state with a weight of 0.08. The calculated values of the $Q$ moment and the polarization charge are $13.0(13.4)e$ fm$^2$ and $e_{\text{pol}}^{\pi} = 0.89e$ (0.96$e$), respectively. The quadrupole moments and polarization charges of $^{31}$Al and $^{33}$Al are not very different.

The dimension of the Hamiltonian (1) is 285 for $^{35}$Al. As in the case of $^{31}$Al and $^{33}$Al, the wave function of $^{35}$Al is written by the one-hole state with a weight of 0.85 and the hole coupled to the $2_1^+$ state with 0.14. The contribution of the coupling to the $2_1^+$ state is larger than that in $^{31,33}$Al. The calculated values of the $Q$ moment and the polarization charge are $14.7(15.1)e$ fm$^2$ and $e_{\text{pol}}^{\pi} = 1.12e$ (1.18$e$), respectively.

To see separately the effects of coupling to the low-lying modes and to the giant resonances on the polarization charge, we diagonalize the Hamiltonian (1) in the model space containing only the RPA modes with energies larger than 10 MeV. The obtained polarization charges for the $1d_{5/2}$ orbital are $e_{\text{pol}}^{\pi} = 0.20e$ (0.22$e$), $0.21e$ (0.24$e$), and $0.18e$ (0.20$e$) in $^{31}$Al, $^{33}$Al, and $^{35}$Al, respectively. These values are close to the systematic value obtained in Ref. [27] (0.21$e$, 0.18$e$, and 0.15$e$ in $^{31,33,35}$Al), where the microscopic PVC calculations
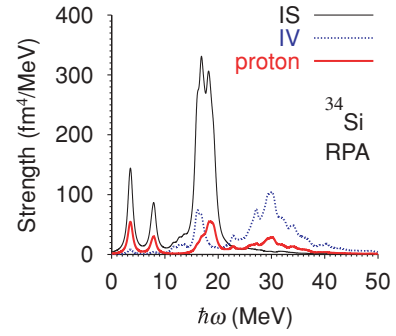


FIG. 3. (Color online) Same as Fig. 1 but for the RPA strengths in $^{34}$Si.

were performed including only the giant resonances on top of the self-consistent HF + RPA in light neutron-rich nuclei.

The enhancement of the polarization charge in $^{35}$Al is thus due to the strong collectivity of the low-lying quadrupole vibrational mode in the core nucleus $^{36}$Si because the effects of coupling to the giant resonances are not sensitive to the neutron number in the Al isotopes under investigation.

### C. Effects of the pairing correlations in $^{33}$Al

We investigate the effects of coupling to the $pf$-shell in $^{33}$Al. The dominant correlation in the present case is the pairing correlation because the core nucleus $^{34}$Si is calculated to be spherical at the HFB level.

Figure 3 shows the IS, IV, and proton quadrupole transition strengths in $^{34}$Si obtained by solving the Skyrme HF + RPA equations without pairing correlations. The collectivity of low-lying states are tremendously weakened, while the structure of GQR is not very different from that obtained by solving the Skyrme HFB + QRPA equations shown in Fig. 1.

The $2_1^+$ state is constructed dominantly by the $(\pi 2s_{1/2} \otimes 1d_{5/2})$ excitation with a weight of 0.98. The strength $B(\text{IS2}; 0^+ \to 2_1^+)$ has only 237 fm$^4$. Using the RPA transition densities, we diagonalize the Hamiltonian (1) with a dimension of 241. The calculated wave function is mainly generated by the one-hole state with a weight of 0.97 and the hole coupled to the $2_1^+$ state with a weight of 0.02. This state is thus dominantly described by the proton $sd$-shell configurations because the $2_1^+$ state is generated by the proton excitation to the $2s_{1/2}$ orbital.

The resulting $Q$ moment is $11.0(11.4)e$ fm$^2$, and the polarization charge is $e_{\text{pol}}^{\pi} = 0.59e$ (0.65$e$).

The $Q$ moment and the polarization charge in $^{33}$Al are quite sensitive to the neutron pairing correlation at $N = 20$. This is similar to the enhancement mechanism of the $B(E2; 0^+ \to 2_1^+)$ in $^{32}$Mg because the neutron pairing correlation is indispensable for the strong collectivity of the $2_1^+$ state in $^{32}$Mg [29].

### D. $^{32}$Mg as a core

The wave function $|^{33}$Al$\rangle$ can also be constructed by the quasiproton coupled to $^{32}$Mg. The pairing gaps of neutrons
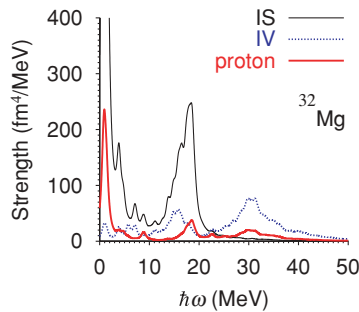
FIG. 4. (Color online) Same as Fig. 1 but in $^{32}$Mg.

and protons are 1.80 and 1.42 MeV in $^{32}$Mg. The ground state is calculated to be spherical as in the other HFB calculations [30,31]. Figure 4 shows the response functions for the IS, IV, and proton quadrupole excitations. At 0.9 MeV, we can see a prominent peak possessing 2414 fm$^4$ and 430 $e^2$ fm$^4$ for the IS quadrupole strength and $B(E2)$, respectively. This result agrees well with the experimental value [9]. The $2_1^+$ state is constructed by the two-quasiparticle excitations of $(\nu 1d_{3/2})^2$ with a weight of 0.10, $(\nu 1f_{7/2})^2$ with 0.09, $(\pi 1d_{5/2} \otimes 2s_{1/2})$ with 0.11, and $(\pi 1d_{5/2})^2$ with 0.61.

We diagonalize the Hamiltonian (1) within the space of the proton quasiparticle of the $1d_{5/2}$ orbital and the coupled states of a $sd$-shell quasiproton to the quadrupole modes in $^{32}$Mg. In the present calculation with a dimension of 276, $|^{33}\text{Al}\rangle$ is constructed by the quasiproton of the $1d_{5/2}$ level with a weight of 0.85, $|\pi 1d_{5/2} \otimes 2_1^+\rangle$ with 0.10, $|\pi 2s_{1/2} \otimes 2_1^+\rangle$ with 0.04, and $|\pi 1d_{3/2} \otimes 2_1^+\rangle$ with 0.01. The electric $Q$ moment of $^{33}$Al is then calculated as 12.4 (12.6) $e$ fm$^2$. This is consistent with the calculation in Sec. III B.

## IV. CONCLUSION

The polarization charges for the electric quadrupole moment of the neutron-rich Al isotopes at around $N = 20$ have been investigated by carrying out the microscopic particle-vibration coupling calculation in which the coordinate-space Skyrme Hartree-Fock-Bogoliubov and quasiparticle random-phase approximations are employed to calculate the single-quasiparticle wave functions and the transition densities.

It has been found that the neutron pairing correlations are crucial to generate the collectivity of the $2_1^+$ state in $^{34}$Si and that the polarization charge of the proton hole state of the $1d_{5/2}$ orbital becomes small in the absence of the pairing correlation in $^{33}$Al. The effect of the neutron pairing correlation at $N = 20$ on the enhancement of the polarization charge in $^{33}$Al is very similar to the enhancement mechanism of the $B(E2)$ in $^{32}$Mg [29].

The effects of coupling to the giant resonances on the polarization charge are not very different in a small region of isotopes, and the low-lying collective modes have much effect on the polarization charge. Therefore, the polarization charge in $^{35}$Al is larger than that in $^{31,33}$Al as a consequence of the stronger collectivity of the $2_1^+$ state in $^{36}$Si.

[1] M. Bender and P.-H. Heenen, Rev. Mod. Phys. **75**, 121 (2003).
[2] D. Vretenar, A. V. Afanasjev, G. A. Lalazissis, and P. Ring, Phys. Rep. **409**, 101 (2005).
[3] N. Paar, D. Vretenar, E. Khan, and G. Colò, Rep. Prog. Phys. **70**, 691 (2007).
[4] D. Peña Arteaga and P. Ring, Prog. Part. Nucl. Phys. **59**, 314 (2007).
[5] S. Péru and H. Goutte, Phys. Rev. C **77**, 044313 (2008).
[6] K. Yoshida and N. V. Giai, Phys. Rev. C **78**, 064316 (2008).
[7] C. Détraz *et al.*, Phys. Rev. C **19**, 164 (1979).
[8] D. Guillemaud *et al.*, Nucl. Phys. **A426**, 37 (1984).
[9] T. Motobayashi *et al.*, Phys. Lett. **B346**, 9 (1995).
[10] P. Himpe *et al.*, Phys. Lett. **B643**, 257 (2006).
[11] V. Tripathi *et al.*, Phys. Rev. Lett. **101**, 142504 (2008).
[12] D. Nagae *et al.*, Phys. Rev. C **79**, 027301 (2009).
[13] T. Nagatomo *et al.*, in *Proceedings of the 5th International Conference on Exotic Nuclei and Atomic Masses*, Ryn, Poland, 7–13 September, 2008 (submitted for publication).
[14] E. K. Warburton, J. A. Becker, and B. A. Brown, Phys. Rev. C **41**, 1147 (1990).
[15] A. Bohr and B. R. Motteleson, *Nuclear Structure* (Benjamin, Elmsford, NY, 1975/World Scientific, Singapore, 1998), Vol. II.
[16] D. M. Brink and R. A. Broglia, *Nuclear Superfluidity: Pairing in Finite Systems* (Cambridge University Press, Cambridge, UK, 2005).
[17] I. Hamamoto, Phys. Rep. **10**, 63 (1974).
[18] P. F. Bortignon, R. A. Broglia, D. R. Bes, and R. Liotta, Phys. Rep. **30**, 305 (1977).
[19] H. Sagawa and B. A. Brown, Nucl. Phys. **A430**, 84 (1984).
[20] I. Hamamoto and H. Sagawa, Phys. Rev. C **54**, 2369 (1996).
[21] N. Van Giai and H. Sagawa, Phys. Lett. **B106**, 379 (1981).
[22] J. Bartel, P. Quentin, M. Brack, C. Guet, and H.-B. Håkansson, Nucl. Phys. **A386**, 79 (1982).
[23] W. Satuła, J. Dobaczewski, and W. Nazarewicz, Phys. Rev. Lett. **81**, 3599 (1998).
[24] K. Mizuyama, M. Matsuo, and Y. Serizawa, Phys. Rev. C **79**, 024313 (2009).
[25] Y. Utsuno, T. Otsuka, T. Mizusaki, and M. Honma, Phys. Rev. C **60**, 054315 (1999).
[26] R. W. Ibbotson *et al.*, Phys. Rev. Lett. **80**, 2081 (1998).

[27] T. Suzuki, H. Sagawa, and K. Hagino, Phys. Rev. C **68**, 014317 (2003).

[28] S. Nummela *et al.*, Phys. Rev. C **63**, 044316 (2001).

[29] M. Yamagami and N. Van Giai, Phys. Rev. C **69**, 034301 (2004).

[30] J. Terasaki, H. Flocard, P.-H. Heenen, and P. Bonche, Nucl. Phys. **A621**, 706 (1997).

[31] R. Rodoríguez-Guzmán, J. L. Egido, and L. M. Robledo, Nucl. Phys. **A709**, 201 (2002).